

## ARTICLE OPEN



# Mitochondrial DNA damage triggers spread of Parkinson's disease-like pathology

Emilie Tresse<sup>1</sup>, Joana Marturia-Navarro<sup>1</sup> , Wei Qi Guinevere Sew<sup>1</sup>, Marina Cisquella-Serra<sup>1</sup>, Elham Jaber<sup>1</sup>, Lluís Riera-Ponsati<sup>1</sup> , Natasha Fauerby<sup>1</sup>, Erling Hu<sup>1</sup>, Oliver Kretz<sup>2</sup>, Susana Aznar<sup>3</sup> and Shohreh Issazadeh-Navikas<sup>1</sup>

© The Author(s) 2023

In the field of neurodegenerative diseases, especially sporadic Parkinson's disease (sPD) with dementia (sPDD), the question of how the disease starts and spreads in the brain remains central. While prion-like proteins have been designated as a culprit, recent studies suggest the involvement of additional factors. We found that oxidative stress, damaged DNA binding, cytosolic DNA sensing, and Toll-Like Receptor (TLR)4/9 activation pathways are strongly associated with the sPDD transcriptome, which has dysregulated type I Interferon (IFN) signaling. In sPD patients, we confirmed deletions of mitochondrial (mt)DNA in the medial frontal gyrus, suggesting a potential role of damaged mtDNA in the disease pathophysiology. To explore its contribution to pathology, we used spontaneous models of sPDD caused by deletion of type I IFN signaling (*Ifnb<sup>-/-</sup>/Ifnar<sup>-/-</sup>* mice). We found that the lack of neuronal IFN $\beta$ /IFNAR leads to oxidization, mutation, and deletion in mtDNA, which is subsequently released outside the neurons. Injecting damaged mtDNA into mouse brain induced PDD-like behavioral symptoms, including neuropsychiatric, motor, and cognitive impairments. Furthermore, it caused neurodegeneration in brain regions distant from the injection site, suggesting that damaged mtDNA triggers spread of PDD characteristics in an "infectious-like" manner. We also discovered that the mechanism through which damaged mtDNA causes pathology in healthy neurons is independent of Cyclic GMP-AMP synthase and IFN $\beta$ /IFNAR, but rather involves the dual activation of TLR9/4 pathways, resulting in increased oxidative stress and neuronal cell death, respectively. Our proteomic analysis of extracellular vesicles containing damaged mtDNA identified the TLR4 activator, Ribosomal Protein S3 as a key protein involved in recognizing and extruding damaged mtDNA. These findings might shed light on new molecular pathways through which damaged mtDNA initiates and spreads PD-like disease, potentially opening new avenues for therapeutic interventions or disease monitoring.

*Molecular Psychiatry* (2023) 28:4902–4914; <https://doi.org/10.1038/s41380-023-02251-4>

## INTRODUCTION

PD is the most common motor neurodegenerative disease. It is a multifactorial pathology with complex etiology mainly characterized by the loss of neurons in the Substantia Nigra (SN) [1]. Even though the exact cause of the neuronal death remains unknown, dysfunctional mitochondria is suggested to play a detrimental role. Neurons have high energy demands due to their elongated morphology [2] and their physiological functions, including membrane-gradient restoration after action potential [3] and recycling of neurotransmitters [4]. Neuronal energy is provided by mitochondria through oxidative metabolism. Genetic studies on familial PD have described monogenic forms with disease-causing mutations in several genes leading directly to mitochondrial dysfunction, including PARK2 (encoding Parkin), PARK6 (encoding Pink1), PARK8, and PARK7 (encoding DJ1) [5–10].

Due to their ancestral endosymbiotic origin, mitochondria possess their own DNA (mtDNA) which, similarly to bacterial DNA, is circular and rich in unmethylated CpG motifs. In mammals, it encodes 13 proteins of the respiratory chain, while most of the proteins involved in mitochondrial homeostasis are encoded by the nuclear genome.

To balance the pool of mtDNA molecules over the number of mitochondria and cellular energy needs, mitochondrial homeostasis and mtDNA biogenesis and maintenance are tightly co-regulated [11, 12]. Upon damage, mtDNA is degraded through mitophagy [13]. Since mtDNA is essential for energy production by the respiratory chain and is therefore critical for neuronal welfare, mtDNA alterations could lead to neurodegeneration.

Genetic variations of mtDNA increase with age [14] and are reported to be associated with PD [14, 15] albeit with conflicting outcomes. These discrepancies may be attributed to the diverse pathology observed in PD and PDD and the differences in brain regions investigated [14, 16–20]. Nevertheless, strong evidence from PD animal models supports the involvement of mitochondrial disturbances including mtDNA packaging [21]. However, there is a large gap in our understanding of the molecular chain of events underlying mitochondrial dysfunctions, their impact on the nature of mtDNA and how damages to mtDNA can further trigger PD pathology and its spread leading to the clinical manifestations.

Interferon-beta (IFN $\beta$ ) is a neuroprotective cytokine, which plays a central role in viral infection [22, 23], treatment of Multiple

<sup>1</sup>Neuroinflammation Unit, Biotech Research & Innovation Centre (BRIC), Faculty of Health and Medical Sciences, University of Copenhagen, Copenhagen Biocentre, Ole Maaløes Vej 5, DK-2200 Copenhagen N, Denmark. <sup>2</sup>Department of Medicine, University Medical Center Hamburg-Eppendorf, Hamburg, Germany. <sup>3</sup>Centre for Neuroscience and Stereology, University Hospital Bispebjerg-Frederiksberg, 2400 Copenhagen, Denmark. ✉email: shohreh.issazadeh@bric.ku.dk

Received: 5 January 2023 Revised: 4 September 2023 Accepted: 5 September 2023

Published online: 2 October 2023

Sclerosis (MS) [24] cerebral ischemia [25, 26] and also in preventing neurodegeneration [27, 28]. In sporadic PD patients, dysregulated IFN $\beta$  signaling was identified as the top candidate pathway associated with disease and its progression to dementia, and subsequent meta-analysis of GWAS recognized sequence variants in IFN $\beta$ -IFNAR signaling pathway related genes [28]. Accordingly, mice knock-out for *Ifnb* or *Ifnar1* develop Parkinson-like disease with dementia (PDD) [27]. This is accompanied with proteinopathy, neurodegeneration including dopaminergic neuron death, and autophagy deficiency [27]. Interestingly, removal of the major accumulated protein associated with PD,  $\alpha$ -synuclein ( $\alpha$ -syn), still allowed proteinopathy and Parkinson-like phenotypes to develop, emphasizing a central role for IFN $\beta$  in preventing PD pathological features [29]. Using the PD *Ifnb*<sup>-/-</sup> mouse model, we have previously demonstrated that neuronal IFN $\beta$  is necessary for maintaining mitochondrial homeostasis and metabolism [30]. Lack of neuronal IFN $\beta$  [30] or perturbation of its downstream signaling [28, 31] causes accumulation of damaged mitochondria with excessive oxidative stress and insufficient ATP production [30].

Our current study reveals that PDD patients with defective type I IFN signaling [28] display dysregulated transcriptomic pathways related to oxidative stress, damaged DNA binding, and cytosolic DNA sensing. Investigating another cohort of PDD patients revealed mtDNA deletions in complex I respiratory chain subunits. To understand the role of IFN in mtDNA damages and PD pathology, we used *Ifnb*/*Ifnar1* deleted mice. We demonstrate that neuronal IFN $\beta$ -IFNAR1 signaling deficiency leads to mtDNA damage and its extrusion both intra-cytoplasmically and extra-neuronally. Injecting damaged mtDNA into healthy mouse brain causes PDD-like pathology and motor and cognitive impairments, while healthy mtDNA does not. Damaged mtDNA also spreads the pathology to other brain regions. This occurs through TLR4 and TLR9 activation, via TLR4-activator protein, Ribosomal Protein S3 (Rps3) [32] that plays a key role in mtDNA damage recognition, extrusion, and neurotoxicity.

## MATERIALS AND METHODS

Detailed information is found in supplementary materials.

### Human brain samples

Human brain samples from healthy controls (NCs) ( $N = 7$ , 3 females and 4 males) and sPD patients ( $N = 7$ , 3 females, 4 males) were collected from the medial frontal gyrus, a region implicated in cognitive impairments in PD [33, 34]. The samples were obtained from the Harvard Brain Tissue Resource Center, USA, Bispebjerg Hospital Brain Bank, Copenhagen, Denmark, and Netherlands Brain Bank with appropriate ethical approvals. Diagnoses were confirmed by postmortem pathology.

For microarray analysis, publicly available data from Parkinson's disease dementia (PDD) and without dementia (PD/PDND), and healthy controls (HC) were used as reported [28].

### Mice

*Ifnb*<sup>-/-</sup> or *Ifnar1*<sup>-/-</sup> mice in C57BL6 background were utilized as models for PD [27, 28] and compared to their littermates/wildtype (also referred to *Ifnb*<sup>+/+</sup>/*Ifnar1*<sup>+/+</sup>/WT). Experiments followed the Danish ethical license 2018-15-0201-01572. All injections and behavioral tests were performed in a randomized double-blind manner.

### mtDNA sequencing by MitoSV-seq

mtDNA sequencing was performed and analysed using the MitoSV-seq method on DNA extracted from Dopaminergic Neurons (DN) FACS-purified from 6-week-old mouse brain as described previously [35].

### mtDNA injection

mtDNA was isolated from wild-type, *Ifnb*<sup>-/-</sup> or *Ifnar1*<sup>-/-</sup> primary cortical neurons [27] using the DNA blood and tissue kit (Qiagen) from mitochondria fraction obtained as described earlier [30]. mtDNA was injected in 10-week-old C57BL/6 mice. By using a stereotactic instrument,

2  $\mu$ L of a 10 ng/ $\mu$ L mtDNA solution were injected using a 10  $\mu$ L Hamilton syringe on both sides in the Frontal Cortex (A/P + 1,8; M/L 1,0; D/V 2,5), the Substantia Nigra (A/P -3,0; M/L 1,3; D/V -3,9) and the Striatum (A/P 0,3; M/L 2,3; D/V -2,9) relative to the bregma. The mtDNA solution was infused at 2  $\mu$ L/min. Eight mice per group were used [29]. Behavior was studied as described previously [27–29], 15 and 30 days post injection. Mice were euthanized 1-month post-injection of mtDNA and brains were collected for further assessment [27–29].

### Cell culture and treatments

Primary cortical neuron (CN) cultures were obtained from cortices of 0–1-day-old pups, dissociated with Papain (2 mg/mL) and single cell suspended using a Pasteur pipette carefully. Cells were cultured in poly-D-lysine hydrobromide coated dishes with Buffer B.

Immortalized Mouse Embryonic Fibroblasts (MEFs), NTC and *Ifnb*<sup>-/-</sup> Neuro2A (N2A) neuroblastoma cell line were generated as described earlier [30].

*mtDNA treatment* in vitro: N2As or CNs (DIV7–9) were treated for 24 h with 30 ng/mL of WT or *Ifnb*<sup>-/-</sup> mtDNA.

*Knock-down*: N2As and CNs were transfected with the respective siRNAs (siRps3 or siTLR4) using Lipofectamine RNAiMAX (Invitrogen 13778030).

*Inhibitors*: ODN-2088 (InvivoGen Catalog code: tlr1-2088) was used at a final concentration of 2.5  $\mu$ M, LPS-rs1 (InvivoGen #tlrl-prslps) at 0.5 ng/mL and RU.521 (InvivoGen cat. Inh-ru521) at 0.5 ng/mL for 24 h according to manufacturer's protocol (Supplementary table 1).

### Western Blotting (WB)

WB was performed as described [30] using the antibodies listed in Supplementary Table 2.

### qPCR

qPCR was performed as described [30] using primers in Supplementary Table 3.

### Immunostaining

Immunostainings and imaging were performed as described [30]. Antibodies and concentration used are listed in Supplementary Table 2.

### Electron microscopy (EM)

Sample preparation details in Supplementary. Images were acquired with a Philips CM 100 Transmission EM (Philips, Eindhoven, The Netherlands) at an accelerating voltage of 80 kV [30].

### Extracellular Vesicles (EVs) purification

EVs were purified from CN culture medium, using the ExoEasy kit (Qiagen). EVs were then pelleted by ultracentrifugation at 160,000  $g$  for 2 h at 4  $^{\circ}$ C and resuspended in culture medium for EV treatment or in lysis buffer for protein analysis or in PBS for DNA purification.

From brain tissue, EVs were purified from freshly collected tissue as described [36].

### EVs Mass Spectrometry and proteomic analysis

Purified EVs were resuspended in Guanidine buffer and run at DTU Proteomics facility for LC-MS. Differential expression proteomics analysis was performed using DEP package (Bioconductor) in RStudio (version 1.4.1106 with R version 4.0.4).

### Immunoprecipitation (IP)

*mtDNA/Rps3*: Neuro2A cells were cultured until 80% confluency, medium was removed, and cells were cross-linked in 1% PFA. Cells were lysed in RIPA, quantified and immunoprecipitated with 30  $\mu$ L of pre-cleared Protein G Sepharose 4 Fast Flow beads and 6  $\mu$ L anti-Rps3 ON at 4  $^{\circ}$ C. After washes DNA was eluted in 1% SDS, 100 mM NaHCO $_3$ , crosslink was reversed with NaCl and DNA was purified and assessed by qPCR.

*Rps3/TLR4*: IP was performed as described [37] using anti-Rps3 antibody (4  $\mu$ g/mL).

### Statistics

For all graphs, 1 dot means 1 individual patient, animal or independent biological replicate. € means  $p < 0.05$ , €€  $p < 0.01$ , €€€  $p < 0.001$ , and €€€€

$p < 0.0001$  for ANOVA, ordinary one-way ANOVA, Kruskal–Wallis ANOVA if distribution did not show Gaussian distribution (Shapiro–Wilk test) or Brown–Forsythe ANOVA if distribution showed SD differences (Bartlett's test). \* means  $p < 0.05$ , \*\*  $p < 0.01$ , \*\*\*  $p < 0.001$ , and \*\*\*\*  $p < 0.0001$  for t-test.

## RESULTS

### Lack of IFN $\beta$ /IFNAR signaling causes mtDNA oxidization and mutation in a hotspot in complex I respiratory chain subunits mimicking PD brain pathology

We analyzed transcriptomic datasets from sPD patients [28] to identify molecular pathways related to the disease pathology. Dysregulated oxidative phosphorylation (OXPHOS) emerged as the top-ranked pathway in sPDD, patients with reported defective type I IFN-signaling [28], compared to HC (Fig. 1A, Supplementary tables 4, 5). This OXPHOS dysregulation was also observed in sPD patients compared to HC (Supplementary table 6). OXPHOS is a crucial neuronal process for energy generation, and its imbalance can lead to excessive production of Reactive Oxygen Species (ROS), causing oxidative mtDNA mutations and damages.

In post-mortem brain samples from another cohort of sPD patients, we observed a loss of ND4 and ND5 (Fig. 1B), which are subunits of the respiratory chain responsible for OXPHOS and are encoded in mtDNA. This finding suggested a potential role of damaged mtDNA in the disease. To investigate this further, we used sPDD-murine models lacking IFN $\beta$ -IFNAR signaling, which resemble the sPDD patients [27, 28]. In *Ifnb*<sup>-/-</sup> neurons, down-regulation of OXPHOS was the top 7th KEGG pathway (Fig. S1A), and brain samples of both *Ifnb*<sup>-/-</sup> and *Ifnar1*<sup>-/-</sup> confirmed the presence of deletions in ND4 and ND5 (Fig. 1C).

*Ifnb*<sup>-/-</sup> neurons exhibited high ROS levels, likely due to defective mitochondrial fission and impaired mitophagy, leading to increased oxidative DNA damages, such as 8-Hydroxyguanosine (8-OHdG) [30]. Immunolabeling of brain tissues from *Ifnb*<sup>-/-</sup> mice showed positive 8-OHdG puncta localized with or near mitochondria, but not in wild-type/*Ifnb*<sup>+/+</sup> brains (Fig. 1D), suggesting increased mtDNA oxidation. Quantification of mtDNA in different brain regions of *Ifnb*<sup>-/-</sup> mice revealed significant loss in the D-loop and *Nd4* regions, containing a more stable DNA region vs. a more susceptible to damages respectively [38], already at 6-week-old mice (Fig. 1E, F), indicating mtDNA alterations especially in the brainstem. These findings reinforce the resemblance of these sPD-models to the neuropathology observed in patients with PD, encompassing regions beyond the basal ganglia [39, 40]. To determine the extent of these damages, we isolated DN from *Ifnb*<sup>+/+</sup> and *Ifnb*<sup>-/-</sup> mice using Flow Cytometry and sequenced their mtDNA by MitoSVseq [35] (Fig. 1G–K, Fig. S1B and Supplementary tables 7–9). We observed a significant loss of DN in the brains of 6-month-old mice, while the number of DN was similar in 6-week-old mice (Fig. 1G, H). Next, the loss of mtDNA was confirmed in DN already in 6-week-old mice, demonstrating that alterations of mtDNA precede DN loss in the *Ifnb*<sup>-/-</sup> sPDD-model, which is observed from 3-month-old mice [27]. Sequencing revealed an accumulation of mutations in mtDNA from *Ifnb*<sup>-/-</sup> DN, in a hot-spot encompassing *Nd4* and *Nd5* encoding genes (Fig. 1J). *Ifnb*<sup>-/-</sup> mtDNA showed a large range of variations, presenting with 28% Single Nucleotide Polymorphisms (SNP), 31% deletions, and 33% inversions (Fig. 1K and Fig. S1B). Similar mtDNA alterations were observed in DN extracted from *Ifnar1*<sup>-/-</sup> brains [35], particularly accumulating in *Nd4* and *Nd5* (Fig. S1C).

These data strongly indicate that dysregulated OXPHOS and mtDNA deletions in brains of sPD patients are co-associated with defects in type I IFN. Lack of IFN $\beta$ -IFNAR signaling leads to oxidization and indel mutations in mtDNA of DN, an early event prior to exhibition of the PDD-like manifestation in *Ifnb1*<sup>-/-</sup> and *Ifnar1*<sup>-/-</sup> mice. These alterations are associated with loss of the key complex I subunits from the electron transport chain, ND4 and ND5, mirroring the findings in patients with PD.

### Damaged mtDNA is extruded from cells lacking IFN $\beta$ /IFNAR

Supporting our mtDNA-related findings, we observed the damaged DNA binding Gene Ontology (GO)-pathway as the 5th downregulated signaling in sPD patients, and cytosolic DNA sensing responses among KEGG-pathways as the 16th upregulated in sPDD (Fig. 2A, B, Supplementary tables 10–13). To explore the nature of damaged mtDNA due to the loss of IFN $\beta$ -IFNAR signaling, we stained *Ifnb*<sup>+/+</sup> and *Ifnb*<sup>-/-</sup> MEFs using an anti-DNA antibody alongside anti-HSP60, although not exclusive, a widely used mitochondrial marker [30, 41, 42]. Surprisingly, in *Ifnb*<sup>-/-</sup> MEFs, 15% of the mtDNA puncta were found outside of mitochondria (Fig. 2C, D), indicating that *Ifnb*<sup>-/-</sup> cells release mtDNA into the cytoplasm. This extruded intracytoplasmic DNA in MEFs was confirmed not to be nuclear (nu)DNA (Fig. S2A–C). 3D reconstruction of EM images of brain tissue [30] further revealed a significantly higher percentage of mitochondria from *Ifnb*<sup>-/-</sup> neurons extruding vesicular structures compared to WT neurons (Fig. 2E, F), with the size resembling mitochondrial-derived vesicles (MDVs) [43] (Fig. 2G). In both *Ifnb*<sup>-/-</sup> and *Ifnar1*<sup>-/-</sup> CNs, mtDNA was enriched in the cytosolic fraction (Fig. S2D). Furthermore, the conditioned medium (CM) [44] from *Ifnb*<sup>-/-</sup> CNs contained significantly more mtDNA, which was oxidized as evidenced by an increase in 8-OHdG levels (Fig. 2H, I). Purified Extracellular Vesicles (EVs) from *Ifnb*<sup>-/-</sup> CN CM or from *Ifnb*<sup>-/-</sup> brainstem also contained higher levels of mtDNA compared to wild-type (Fig. 2J, K). This mtDNA in *Ifnb*<sup>-/-</sup> brain showed a heavy load of alterations (Fig. 2L), as observed earlier.

In conclusion, our results provide evidence that neurons lacking IFN $\beta$ /IFNAR1 are extruding damaged mtDNA in EVs likely originating from mitochondria.

### Damaged mtDNA is pathogenic, induces neurodegeneration and clinical deficits like PDD

We examined the impact of extruded altered mtDNA on neuronal homeostasis in vitro and in vivo. Treating healthy wild-type primary neurons with damaged mtDNA from *Ifnb*<sup>-/-</sup> neurons (KOmtDNA) induced neuronal cell-death, while nuDNA at the same concentration did not have the same effect (Fig. 3A). Similar results were observed in N2A cells (Fig. S3A). Remarkably, only KO damaged mtDNA, not an equivalent concentration of WTmtDNA, or even higher doses (up to 300 ng/mL) elicited the same neuronal death response (Fig. S3B, C). This contradicts previous reports suggesting that undamaged mtDNA can cause cellular toxicity. However, these effects were observed at doses much higher (up to 100 times) [45, 46] than those used in our study. Furthermore, KOmtDNA induced neuronal loss in both healthy and *Ifnb*<sup>-/-</sup> neurons (Fig. S3C–E). Thus, damaged mtDNA-induced neuronal death does not require endogenous IFN $\beta$ -IFNAR signaling for its detrimental mode of action. Interestingly, even WTmtDNA increased neuronal death and astrogliosis in vulnerable *Ifnb*<sup>-/-</sup> neurons (Fig. S3D, E). These results were confirmed by the assessment of primary neurons' viability, where only damaged *Ifnb*<sup>-/-</sup> mtDNA treatment decreased MTT levels. Treating primary neurons with *Ifnb*<sup>-/-</sup> CM, containing EVs with damaged mtDNA, had a similar impact (Fig. 3B). In addition, treatment with damaged KOmtDNA increased oxidative stress by elevating oxidized deglycase-1, (ox)DJ1 [28, 30], in healthy WT neurons, while WTmtDNA did not impact DJ1 oxidation (Fig. 3C).

Moving to in vivo experiments, we injected mtDNA extracted from WT, *Ifnb*<sup>-/-</sup>, or *Ifnar1*<sup>-/-</sup> neurons into the brains of WT mice (Fig. 3D) and assessed their motor, neuropsychiatric, and cognitive abilities one month later. While there were no differences in weight observed, mice injected with damaged KOmtDNA showed impaired performance in motor tasks compared to those injected with mtDNA from WT neurons (Fig. 3E, Fig. S3F–H). They also exhibited increased climbing time and climbing events, potentially related to anxiety (Fig. 3F, Fig. S3I). In a Barnes Maze test, mice injected with damaged KOmtDNA required more time to

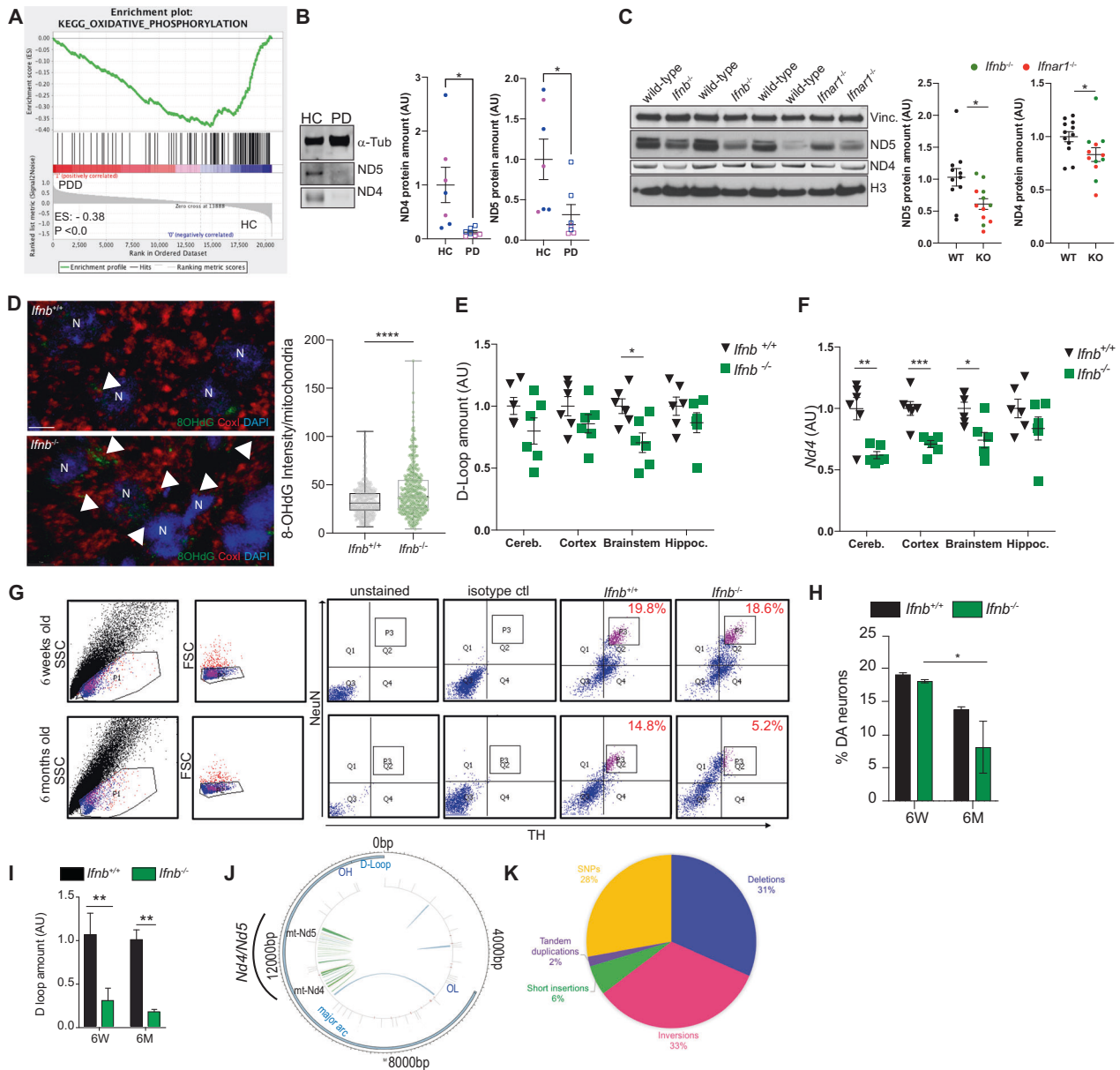


**Fig. 1** Complex I respiratory chain subunits are altered in PD patients and PD models ( $Ifnb^{-/-}/Ifnar1^{-/-}$ ) due to mtDNA damages. **A** Enrichment plot of KEGG-OXPPOS from microarray data comparing sporadic Parkinson's disease with dementia (spDD/ $N = 13$ ) and healthy controls (HC/ $N = 14$ ). **B** Immunoblot showing loss of ND4 and ND5 proteins in the prefrontal cortex of healthy controls (HC) or Parkinson Disease patients (PD), with quantification. Pink indicates females and blue males. **C** Immunoblot showing loss of ND4 and ND5 proteins in the brainstems of 12-month-old mice, with quantifications. **D** Immunolabelling for 8-OHdG (pseudocoloured green), Coxl (mitochondria, pseudocoloured red) in mice midbrains. DAPI stains nuclei. Scale bars equal 5 microns. Quantification of 8-OHdG as integrated density of 8-OHdG in mitochondria of 3-month-old mice. Each dot represents a mitochondrion assessed ( $N = 415$ ) from 3 biological replicates. **E** qPCR for D-loop in different brain regions in 6-week-old mice. **F** qPCR for major arc based on  $Nd4$  amplification in different brain regions in 6-week-old mice. For **E** and **F** each dot represents one individual animal,  $N = 6$ . **G** FACS cell sorting to isolate single dopaminergic (DN) neurons from midbrain of 6-week and 6-month-old mice. NeuN<sup>+</sup> indicate neurons and NeuN<sup>+</sup>TH<sup>+</sup>, dopaminergic neurons. **H** Quantification of (**G**) in 6-week-old or 6-month-old mice.  $N = 3$ . **I** qPCR for D-loop in single isolated DN. Data are mean  $\pm$  SEM,  $N = 3$  mice/group. **J** Position of SVs and SNVs detected with MitoSV-seq in 6-week-old  $Ifnb^{-/-}$  mice. Circos plots of mouse mtDNA genome displaying Heavy and Light Origin of replication (OH and OL, respectively), major arc and D-loop (outer blue circle). mtDNA genes are displayed in the middle circle (grey lines). SVs as arches with deletions (blue), tandem duplications, inversions and insertions (orange). Thickness of the arches correspond to SVs heteroplasmy. SNVs are marked with short red lines (—) according to their positions in mouse mtDNA. Intensity of red lines correspond to SNVs' heteroplasmy. **K** Pie chart showing the distribution of variation types detected in  $Ifnb^{-/-}$  mice; SNP: Single Nucleotide Polymorphism. For all graphs,  $*$   $p < 0.05$ ,  $**$   $p < 0.01$ ,  $***$   $p < 0.001$ , and  $****$   $p < 0.0001$  by unpaired  $t$ -test.

find the exit-box compared to control mice injected with PBS (Fig. 3G) indicative of cognitive impairments. Staining of brain regions revealed significant neuronal loss, including DN (TH<sup>+</sup>) in striatum/STR and SN, increased cCas3<sup>+</sup>NF200<sup>+</sup> and phosphorylated (p) $\alpha$ -syn<sup>+</sup> proteinopathy associated with damaged

KOmtDNA injection, particularly in the frontal cortex (FC) (Fig. 3H–K), confirmed by immunoblotting of brainstem lysates (SN, STR and thalamus) (Fig. 3L).

Three months post injection, EM revealed inclusion bodies (IB) and an accumulation of lipofuscin granules (LG) associated to

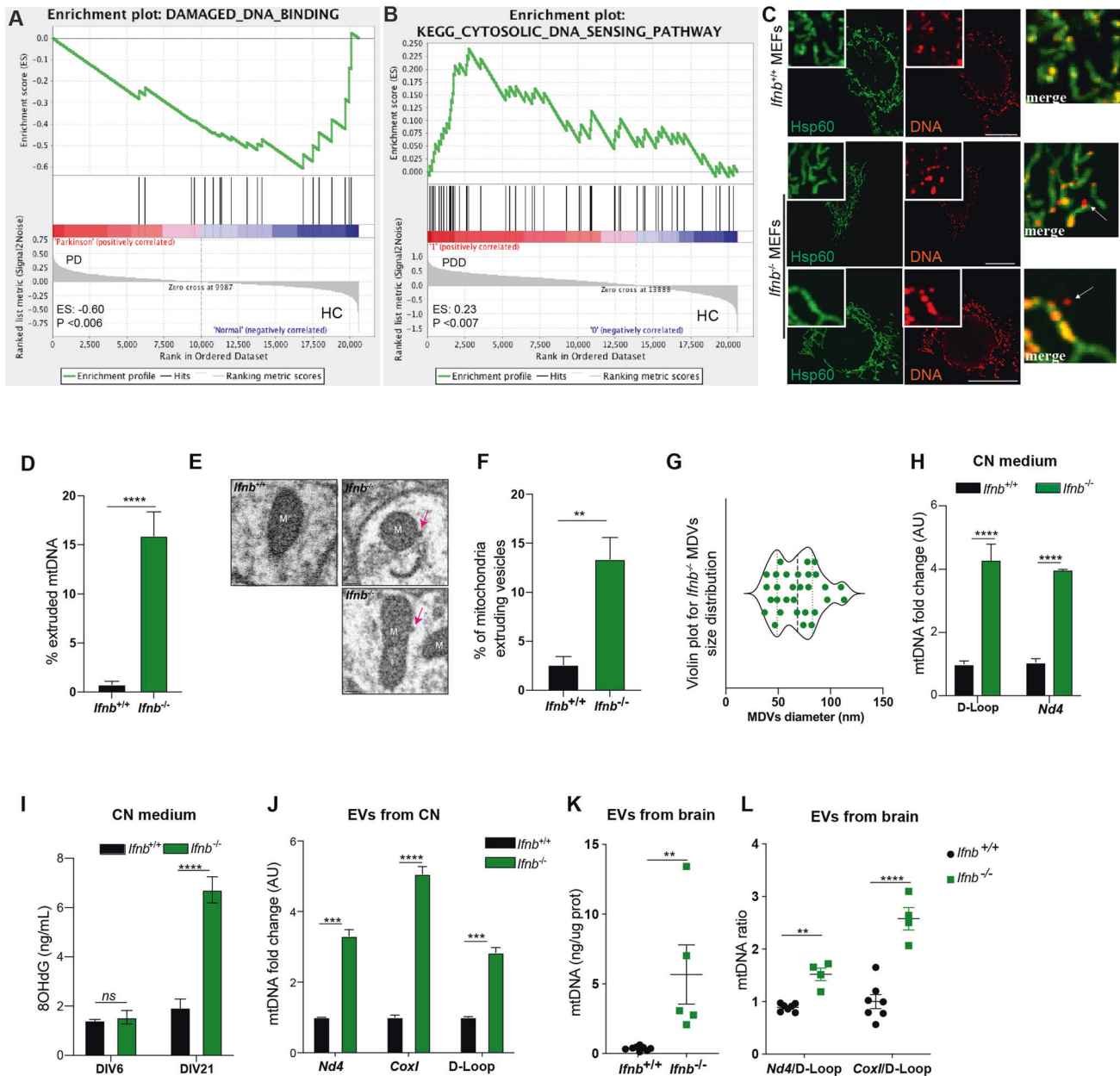


**Fig. 2** mtDNA is extruded in cells lacking IFN $\beta$ . **A** Enrichment plot of GO-Damaged DNA binding, **(B)** Enrichment plot of KEGG-Cytosolic DNA sensing from microarray data comparing sPDD ( $N = 13$ ) and HC ( $N = 14$ ). **C** Immunofluorescence of anti-Hsp60 (mitochondria, pseudocoloured green) and DNA (pseudocoloured red) in MEFs. Extruded mtDNA is indicated with white arrows. Scale bars equal 10 microns. **D** Quantification of extruded mtDNA as % of non-nuclear DNA $^{+}$  puncta not localized in mitochondria.  $N = 3$ . **E** EM showing buds of vesicles being extruded from mitochondria from *Ifnb* $^{-/-}$  thalami. Pink arrows indicate vesicles. Scale bars equal 100 nm. **F** Quantification of % of mitochondria extruding vesicles in thalami.  $N = 10$  EM field/ genotype. **G** Size quantification of vesicles being extruded from mitochondria. **H** qPCR from CM of wild-type or *Ifnb* $^{-/-}$  CN (DIV6) for the mtDNA genes *Nd4* and D-Loop.  $N = 3$ . **I** ELISA of 8-OHdG in CM of CN (DIV6, 21).  $N = 4$ . **J** qPCR for mtDNA *Nd4*, *Cox1* and D-Loop from purified EVs from CN conditioned media (DIV6).  $N = 4$ . **K** Quantification of mtDNA from EVs purified from brainstems of mice.  $N = 4$ . **L** Ratio of *Nd4*/D-Loop and of *Cox1*/D-Loop in mtDNA from EVs purified from brainstems of mice.  $N = 4$ . For all graphs mean  $\pm$  SEM. \*  $p < 0.05$ , \*\*  $p < 0.01$ , \*\*\*  $p < 0.001$ , and \*\*\*\*  $p < 0.0001$  by unpaired  $t$ -test.

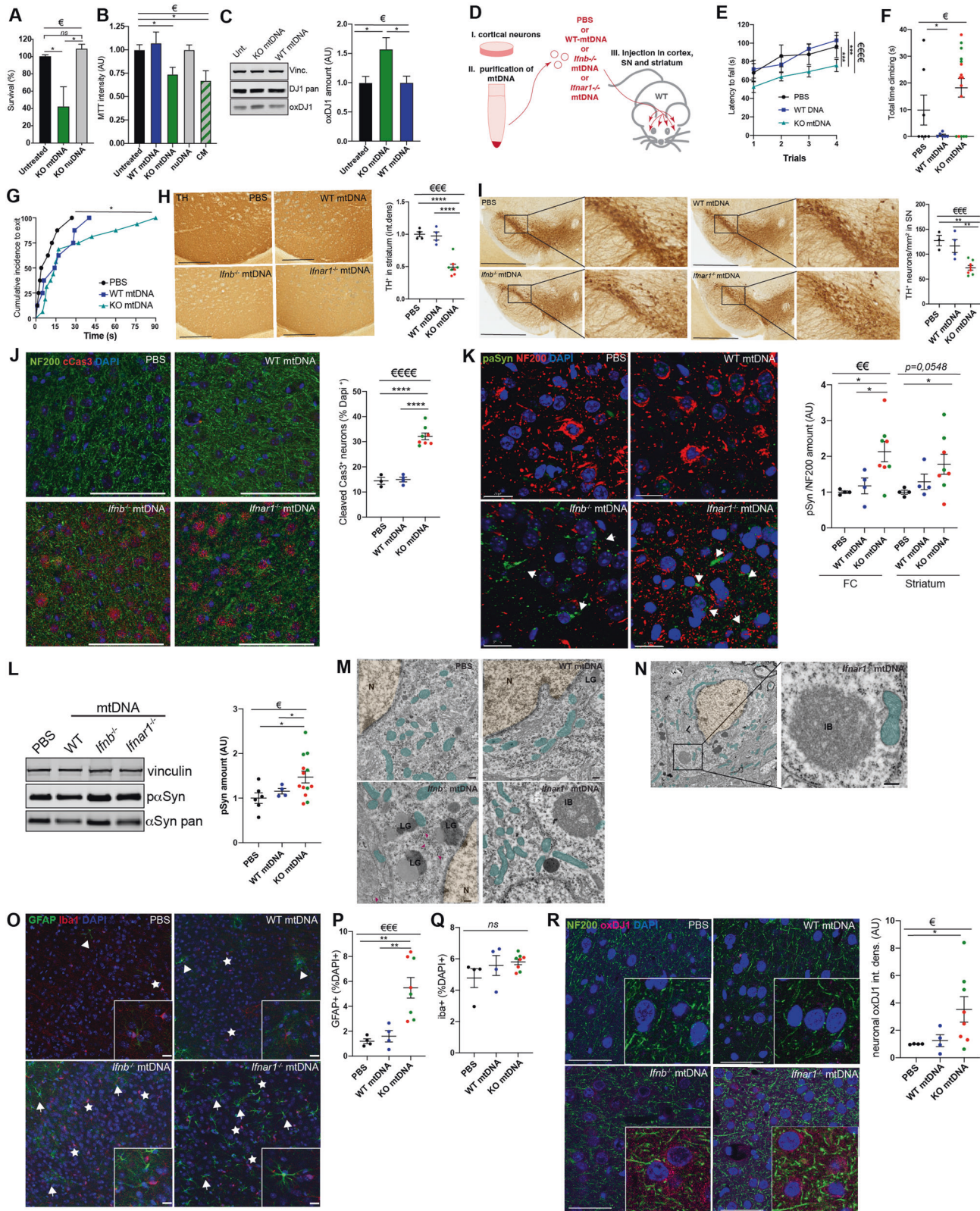
neuromelanin, both pathogenic features of ND, only in the STR of damaged KOMtDNA injected animals (Fig. 3M, N). Furthermore, the mice injected with KOMtDNA displayed astrogliosis, a typical feature of PD [44], in the cortices (Fig. 3O, P). No significant differences in microgliosis (Iba1 $^{+}$ ) were observed between WTmtDNA and KOMtDNA injected groups (Fig. 3O, Q). In addition, injected damaged KOMtDNA resulted in increased oxDJ1 levels in the brain (Fig. 3R, Fig. S3J).

In conclusion, these results demonstrate that damaged and extruded *Ifnb* $^{-/-}$ /*Ifnar1* $^{-/-}$  mtDNA is neurotoxic not only in vitro

but also in vivo, recreating PDD-like pathology and leading to anxiety, motor and cognitive dysfunctions in mice. This is associated with neuronal loss including DNs, accumulation of pa-syn proteinopathy, oxidative stress, and astrogliosis in the injected brain regions.

#### Altered *Ifnb* $^{-/-}$ /*Ifnar1* $^{-/-}$ mtDNA propagates neurodegeneration in distant brain regions

We investigated whether damaged KOMtDNA could propagate pathology to distant brain regions, considering that over 80% of PD patients develop dementia [47], and extended regional



pathology in the brain [33]. The olfactory bulbs (OB) were studied as they are suggested to be primarily affected during PD development [48]. Mice injected with damaged KOmtDNA showed significantly elevated cCas3<sup>+</sup> staining in the OB, indicating active neuronal death (Fig. 4A–C). Immunoblotting confirmed

increased markers of apoptosis, cCas3 and cFLIP, in the OB (Fig. 4D–F). Oxidative stress, indicated by elevated oxDJ1 levels, was also observed in the OB (Fig. 4D, G). Moreover, specific DN loss in the Glomerular Layer (GL) and External Plexiform Layer (EPL) of the OB was significant in mice injected with damaged

**Fig. 3 Damaged mtDNA is neurotoxic in vitro and in vivo.** **A** Survival of CNs assessed by crystal violet staining upon treatment for 24 h with either KOmtDNA or nuDNA.  $N = 3$ . **B** CN metabolism assessed by MTT assay upon treatment for 24 h with either KO or WT mtDNA, nuDNA or CM.  $N = 4$ . **C** Oxidative stress assessed in wild-type CNs upon treatment for 24 h with either WT or KO mtDNA by immunoblot anti-oxDJ1 and quantification.  $N = 6$ . **D** Schematic of injection of mtDNA in mouse brain. **E–G** Motor and cognitive evaluation of mice injected with either PBS (black,  $N = 8$ ), WTmtDNA (blue,  $N = 8$ ), or KOmtDNA (*Ifnb*<sup>-/-</sup> mtDNA: green,  $N = 8$ ; *Ifnar1*<sup>-/-</sup> mtDNA: red,  $N = 8$ ). **E** Rotarod. Statistics calculated from AUC. **F** Cylinder test. **G** Cumulative incidence to find probe during Barnes Maze.  $P\text{-val} = 0,0287$  upon Mantel-Cox statistical assessment. **E–G**  $N = 8$  **H** TH staining in striatum with quantification. Scale bars equal 1 mm. **I** TH staining in SN with quantification. Scale bars equal 500 microns. **J** Immunostaining anti-cCas3, NF200 (neurons) and DAPI (nuclei) in FC and quantification. Scale bars equal 100 microns. **K** Projection of immunostaining anti-p $\alpha$ Syn, NF200 (neurons) and DAPI (nuclei) in FC and quantification. White arrowheads indicate neuronal perinuclear accumulation of p $\alpha$ Syn. Scale bars equal 20 microns. **H–K**  $N = 4$ . **L** Immunoblotting for p $\alpha$ Syn and quantification. Vinculin was used as housekeeping.  $N = 4–6$ . **M, N** EM of injected mice 3 months post-injection. **M** Neuronal cell bodies overview. **N** Enlargement showing an inclusion body at high magnification. For all EM images, scale bars equal 200 nm, nuclei are underlined in orange, mitochondria in teal, LG means Lipofuscin Granules, IB means Inclusion Bodies, purple arrows indicate tangles. **O** Gliosis assessment by immunostaining anti-GFAP (astrocytes, green, white star) and anti-Iba1 (microglia, red, white arrowhead). **P** Quantification of GFAP staining in **(O)**. **Q** quantification of Iba1 staining in **(O)**. **R** Immunostaining for oxDJ1 in FC and quantification. Scale bars equal 50 microns. **O–R**  $N = 4$ . For all graphs, 1 dot means 1 individual animal. PBS is shown in black, WT mtDNA in blue, and KO mtDNA in green (*Ifnb*<sup>-/-</sup> mtDNA) and red (*Ifnar1*<sup>-/-</sup> mtDNA). € means  $p < 0.05$ , €€  $p < 0.01$ , €€€  $p < 0.001$ , and €€€€  $p < 0.0001$  ordinary one-way ANOVA, Krustal-Wallis ANOVA if distribution did not show Gaussian distribution (Shapiro–Wilk test) or Brown-Forsythe ANOVA if distribution showed SD differences (Bartlett's test). \* means  $p < 0.05$ , \*\*  $p < 0.01$ , \*\*\*  $p < 0.001$ , and \*\*\*\*  $p < 0.0001$  by post-hoc unpaired t-test.

KOmtDNA (Fig. 4H). Similar spreading of neuronal death was observed in the cerebellum (Fig. S4). Notably, the spread could likely be due to axonal dopaminergic projections from the SN to the EPL, granule cell layer, and mitral cell layer of the OB, ablation of which impairs olfactory perception [49], and/or the injected solutions could potentially enter the cerebrospinal fluid and reach other brain regions, contributing to the spread of pathology.

These results demonstrate that damaged *Ifnb*<sup>-/-</sup>/*Ifnar1*<sup>-/-</sup> mtDNA not only induces clinical and pathological manifestations of PDD in mice but also propagates the pathology to distant neurons in other brain regions.

#### Upregulated TLR9 in PDD patients and damaged mtDNA-injected brains are related to mitochondrial oxidative stress

To understand the pathological impact of damaged mtDNA due to dysfunctional IFN $\beta$ -IFNAR signaling, we reanalyzed transcriptomic data from sPDD patients and HC [28] for potential molecular mechanisms. We identified the TLR-signaling pathway among the top 20 significant KEGG-pathways associated with sPDD (11th, Supplementary tables 12, 14, Fig. 5A, B). *TLR9* and its downstream signaling protein *IRAK1* were significantly upregulated in sPDD patients compared to HC (Fig. 5C). TLR9 recognizes unmethylated CpG motifs in bacterial DNA and mtDNA [50, 51], we investigated whether TLR9 was activated in response to extruded damaged KOmtDNA. We found modestly increased *Tlr9* expression (Fig. 5D), and *Irak1* mRNA expression significantly upregulated in the brain of mice injected with KOmtDNA compared to controls (Fig. 5E). In primary neurons, *Tlr9* and *Irak1* mRNA were also upregulated upon mtDNA treatment (Fig. 5F, Fig. S5A), indicating a general plausible homeostatic role in neuronal response to free-mtDNA.

To explore the involvement of TLR9 in neuronal dysfunction caused by damaged KOmtDNA, we inhibited TLR9 using a specific antagonist, ODN2088 in cortical neurons. We observed an efficient blockade of the signaling, leading to downregulation of downstream proteins phosphorylated TANK-binding kinase 1 (pTBK1) and phosphorylated Interferon Regulatory Factor 7 (pIRF7), but it did not prevent cell-death in primary neurons (Fig. S5B, D).

In neurons lacking IFN $\beta$  signaling and impaired mitochondrial activity, TLR9 inhibition positively affected mitochondrial health, reducing the production of various ROS species as assessed by DCFDA and MitoSox stainings (Fig. 5G, Fig. S5E, F). In addition, using another selective inhibitor of superoxide production from mitochondrial respiratory complex site III, S3qel, further reduced DCFDA intensity when combined with the TLR9 inhibitor (Fig. S5E). In support, TLR9 inhibition also decreased *Sod2* mRNA and oxDJ1, while increasing the mitochondrial membrane potential in *Ifnb*<sup>-/-</sup> neurons (Fig. S5G–I). Although TLR9 inhibition showed a positive

impact on oxidative stress markers, it did not prevent cell-death or rescue apoptotic cCas3<sup>+</sup> neurons (Fig. 5H, Fig. S5C, D).

Our data support a role for TLR9 in inducing oxidative stress upon recognizing damaged mtDNA, but not in mtDNA-induced neuronal death.

#### TLR4 is upregulated in response to damaged mtDNA and triggers neuronal death

We observed significant upregulation of TLR4 in the transcriptomes of both PD and PDD patient groups (Fig. 5A and I), as well as in the brains of mice injected with damaged mtDNA (Fig. 5J), and primary neurons treated with KOmtDNA (Fig. 5K). To investigate the functional relevance of TLR4 response to damaged mtDNA, we inhibited TLR4 using the antagonist Lipopolysaccharide [52] from the photosynthetic bacterium *Rhodobacter sphaeroides* (LPSrs) (Fig. 5H and S5D–H) and via siRNA knockdown (Fig. 5L, M and S5J, K). The inhibition of TLR4 efficiently prevented neuronal death when wildtype neurons were treated with damaged KOmtDNA (Fig. 5H, Fig. S5D). Notably, inhibition of cytosolic DNA sensor, Cyclic GMP-AMP synthase (cGAS) by using its inhibitor RU521 did not prevent neuronal death mediated by damaged KOmtDNA (Fig. 5H, Fig. S5D), consistent with no significant changes in mRNA or protein levels of cGAS, or impact in wild-type CN treated with damaged KOmtDNA (Fig. S5L, M). These data indicate that TLR4, and not TLR9 or cGAS, is the main driver of damaged mtDNA-induced neuronal death.

To establish the role of TLR4 in oxidative damages in *Ifnb*<sup>-/-</sup> neurons, we successfully knocked down *Tlr4* (Fig. S5J), which interestingly also resulted in decreased *Irak1* expression, and increased neuronal viability compared to the control (Fig. 5L, M), while it did not impact mitochondrial membrane potential (Fig. S5K). These findings suggest that although TLR4 might impact some common downstream signaling as TLR9, it also exerts distinct functions.

In summary, these results demonstrate that damaged mtDNA from cells lacking endogenous IFN $\beta$ -IFNAR signaling induces neuronal cell-death through activation of TLR4, suggesting a new function for TLR4 in response to damaged mtDNA.

#### TLR4 activator Rps3 recognizes damaged mtDNA, an essential step for its extrusion

We utilized a proteomic approach to investigate additional molecular factors that may contribute to the pathogenicity of damaged KOmtDNA in relation to TLR4. As we had previously demonstrated, damaged mtDNA is packed into EVs released by neurons lacking IFN $\beta$  (Fig. 2J–L). These EVs, like pure damaged mtDNA, reduced cell survival in healthy neurons (Fig. 6A). To gain

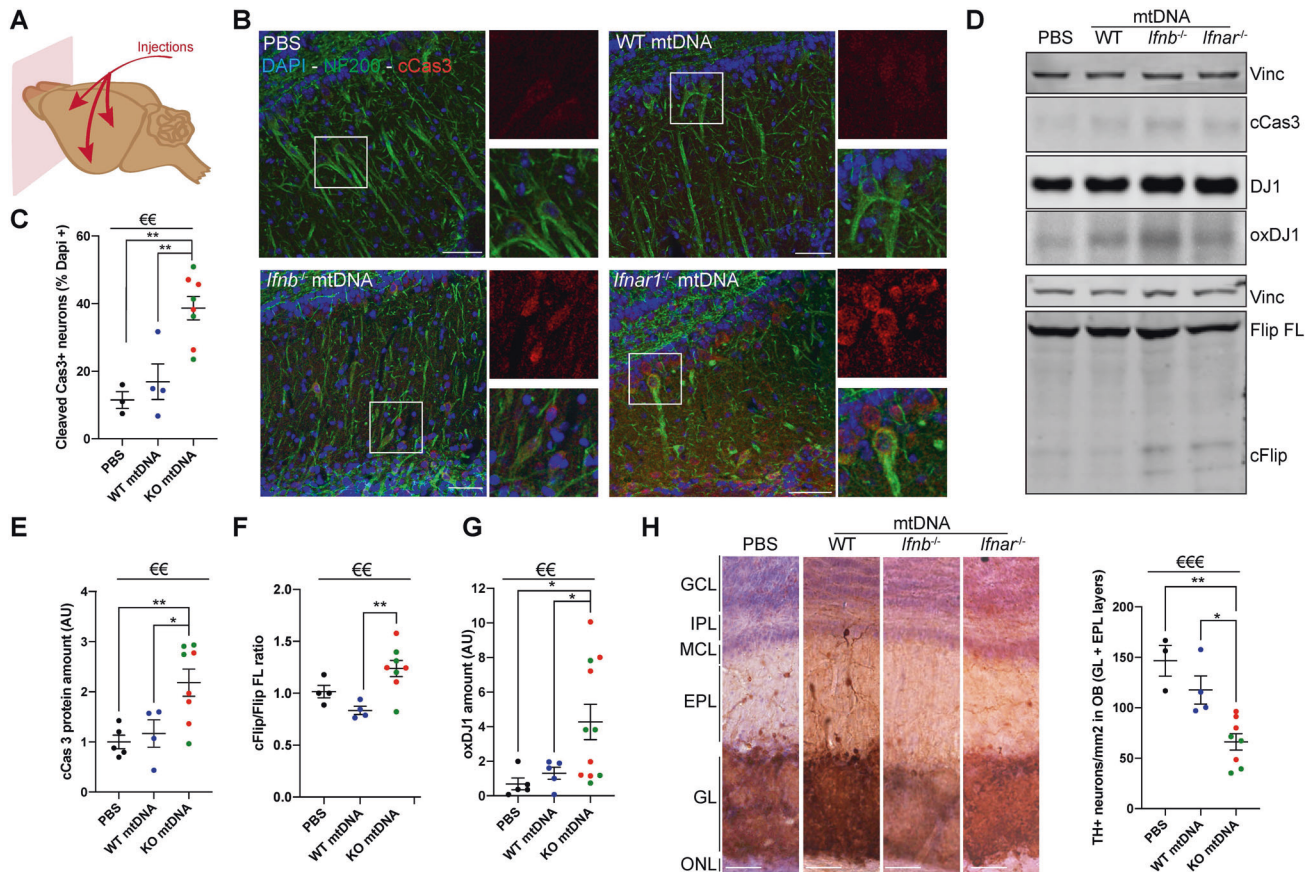


**Fig. 4 Damaged mtDNA spreads neurodegeneration in other part of the brain.** **A** Schematic showing the strategy of investigation in OB. Tissue was evaluated one-month post-injection. **B** Immunofluorescence for cCas3 (red) and NF200 (green, neurons) in OB from injected mice. Scale bars equal 50 microns. **C** Quantification of **(B)**. **D–G** Immunoblots and quantifications of proteins extracted from OB from mice injected with PBS, WTmtDNA, *lfnb*<sup>-/-</sup> mtDNA or *lfnar1*<sup>-/-</sup> mtDNA for cell death markers. **E** cCas3 and **(F)** Flip, and oxidative stress marker **(G)**, oxDJ1. **H** Immunolabelling of TH<sup>+</sup> neurons (reddish brown) with hematoxylin (blue) counterstain in OB from injected mice and quantification. For all graphs, 1 dot means 1 individual animal. PBS is shown in black, WTmtDNA in blue, and KOmtDNA in green (*lfnb*<sup>-/-</sup> mtDNA) and red (*lfnar1*<sup>-/-</sup> mtDNA), *N* = 4–8/group. €€ means *p* < 0.01 and €€€ *p* < 0.001 by ordinary one-way ANOVA, Kruskal-Wallis ANOVA if distribution did not show Gaussian distribution (Shapiro-Wilk test) or Brown-Forsythe ANOVA if distribution showed SD differences (Bartlett's test). \* means *p* < 0.05 and \*\* *p* < 0.01, by post-hoc unpaired *t*-test.

insights into the molecular mechanisms underlying the packaging of damaged mtDNA into EVs and its neurotoxic effects, we purified EVs from both wild-type and *lfnb*<sup>-/-</sup> primary CN CM and subjected them to Liquid Chromatography Mass Spectrometry (LC-MS) analysis (Fig. 6B–E, Fig. S6A–G). By employing an unbiased Label-Free Quantification (LFQ) approach to identify protein changes between *lfnb*<sup>+/+</sup> and *lfnb*<sup>-/-</sup> EVs, we detected a total of 2381 proteins, with 2146 proteins showing High Confidence FDR, indicating a high-quality readout (Fig. S6A). Although the protein abundance was quite similar in all 3 replicates per group, EVs purified from *lfnb*<sup>-/-</sup> neurons revealed a higher number of identified proteins compared to *lfnb*<sup>+/+</sup> neurons (Fig. 6B, Fig. S6D), suggesting that damaged mtDNA is released within a more complex EV pool. Principal Component Analysis (PCA) of the entire dataset and clustering of samples based on genotype in Heatmap (Fig. S6C, D) revealed a specific protein signature in the *lfnb*<sup>-/-</sup> EVs. As expected, we identified EV markers in both *lfnb*<sup>+/+</sup> and *lfnb*<sup>-/-</sup> EVs (Fig. S6E), including L1CAM, a protein known to be enriched in neuronal EVs [53].

Importantly, we found around 300 mitochondria-related proteins in EVs, some showing clear differences between *lfnb*<sup>+/+</sup> and *lfnb*<sup>-/-</sup> populations. For example, Tom70a, a key mitophagy protein [54], was significantly decreased in *lfnb*<sup>-/-</sup> EVs, while HspA9, a marker of MDVs destined for lysosomal degradation [55], was increased in *lfnb*<sup>-/-</sup> EVs (Fig. 6B and S6F).

Notably, DNA repair and TLR modulator pathways were among the top 5 GO terms after GSEA analysis (Fig. 6C; Fig. S6G). One of the proteins highly enriched in *lfnb*<sup>-/-</sup> EVs was Rps3 (Fig. 6B and D). Interestingly, Rps3 was the only protein we identified belonging to TLR4 modulator [32] and Base Excision Repair (BER) pathways, which binds to Apex1 [56], also upregulated in the KO EVs. Furthermore, we identified Rps3 as the only protein in our data set shared among TLR-ligands, mtDNA maintenance, and oxidized DNA binding proteins pathways (Fig. 6C–E, S6D, G and Supplementary table 11). Rps3 is about 20 times more abundant in EVs purified from *lfnb*<sup>-/-</sup> brain tissues as seen by Western Blotting (Fig. 6F).

In KO neurons, we found Rps3 mainly in the cytoplasmic fraction and not in the mitochondrial fraction, while it is found in both fractions in wild-type neurons (Fig. 6G). As Rps3 specifically recognizes 8-OHdG, oxidized alterations on DNA [57], we hypothesized that Rps3 could bind oxidized and damaged mtDNA and be extruded within EVs. Indeed, in a staining of wild-type and *lfnb*<sup>-/-</sup> MEFs we found that Rps3 was outside the mitochondria and colocalized to cytoplasmic mtDNA in *lfnb*<sup>-/-</sup> cells compared to WT (Fig. 6H and Fig. S6H).

To establish if Rps3 binds to oxidized mtDNA, we immunoprecipitated Rps3 from N2A cells followed by qPCR for mtDNA genes. We established that Rps3 directly binds damaged mtDNA in a higher proportion in *δlfnb* cells, but also in



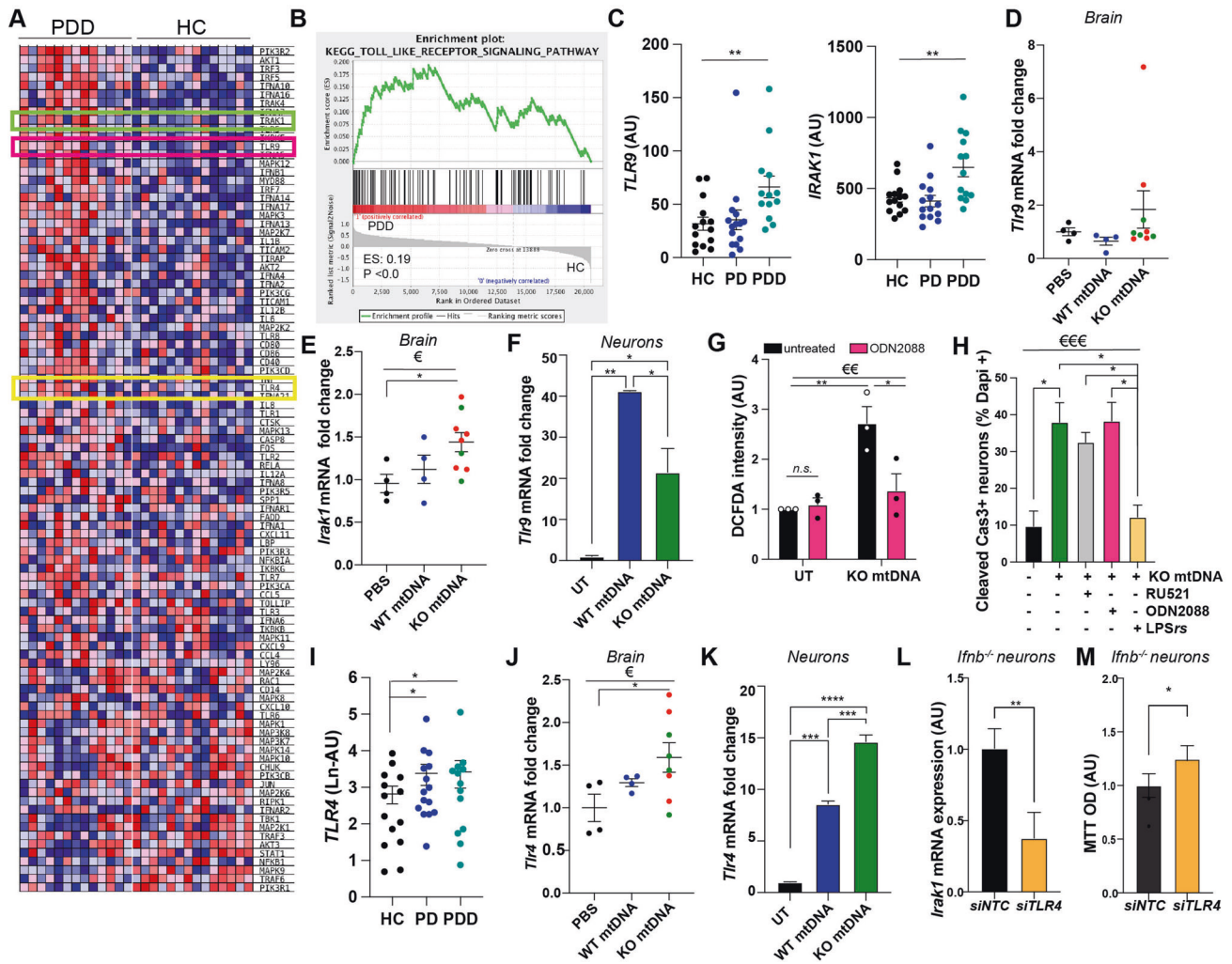


**Fig. 5** TLR9 signalling is upregulated in PDD patient and triggers oxidative stress in neurons, while TLR4 triggers neuronal death. **A** Heat map from GSEA of the TLR signalling pathway and comparing microarray data from sPDD ( $N = 13$ ) and HC ( $N = 14$ ). TLR9 is circled in green and TLR4 in yellow. **B** Enrichment plot of the TLR signalling pathway. **C** Expression of *TLR9* and *IRAK1* in HC and PDD patients extracted from (A). **D**, **E** mRNA levels of (D). *Tlr9* and (E). *Irak1* in mice injected with either PBS ( $N = 4$ ), WTmtDNA ( $N = 4$ ) or KO mtDNA ( $N = 9$ ), (F) mRNA levels of *Tlr9* in primary CNs untreated or treated with either WT mtDNA or KO (*Ifnb*<sup>-/-</sup>) mtDNA. One representative of 3 independent experiments. **G** Normalized DCFDA integrated density quantification wild-type neurons treated with KOmtDNA with or without the presence of TLR9 inhibitor ODN2088. **H** Quantification of cCas3 staining in WT neurons treated with KOmtDNA with or without the presence of cGAS inhibitor RU521, TLR4 inhibitor LPS *rs* or ODN2088. Immunofluorescence staining in S5D. **G**, **H**  $N = 3$ . **I** Expression of TLR4 in HC and PDD patients extracted from (A). **J** mRNA levels of *Tlr4* in mice injected with either PBS ( $N = 4$ ), WTmtDNA ( $N = 4$ ) or KOmtDNA ( $N = 9$ ). **K** mRNA levels of *Tlr4* in primary CNs untreated or treated with either WTmtDNA or KO (*Ifnb*<sup>-/-</sup>) mtDNA. One representative of 3 independent experiments. **L** *Irak1* expression in *Ifnb*<sup>-/-</sup> CNs NTC or knock-down for *Tlr4*. **M** Viability of *Ifnb*<sup>-/-</sup> CNs NTC or knock-down for *Tlr4* assessed by MTT staining. For all graphs, 1 dot means 1 individual animal. For (D, E and J) PBS injected mice are shown in black, WTmtDNA in blue, and KOmtDNA in green (*Ifnb*<sup>-/-</sup> mtDNA) and red (*Ifnar1*<sup>-/-</sup> mtDNA),  $N = 4$ /group. €€ means  $p < 0.01$  and €€€  $p < 0.001$  by ordinary one-way ANOVA, Kruskal–Wallis ANOVA if distribution did not show Gaussian distribution (Shapiro–Wilk test) or Brown–Forsythe ANOVA if distribution showed SD differences (Bartlett’s test). **G** Was analyzed by 2way-ANOVA. \* means  $p < 0.05$  and \*\*  $p < 0.01$ , \*\*\*  $p < 0.001$ , and \*\*\*\*  $p < 0.0001$  by post-hoc unpaired t-test.

wild-type cells treated with a H<sub>2</sub>O<sub>2</sub> pulse as a positive control to induce oxidative damages in mtDNA (Fig. 6I and Fig. S6I). Moreover, we observed a significant increase of Rps3 protein levels in WT CNs treated with damaged KOmtDNA, but not with WTmtDNA (Fig. 6J). To check whether Rps3 could be recognized by and activate TLR4 in neurons, we coimmunoprecipitated TLR4 using an anti-Rps3 antibody (Fig. 6K) showing that these proteins indeed bind. Moreover, knock-down of Rps3 with siRNA (Fig. S6J, K) decreased the amount of damaged mtDNA extruded in EVs purified from either *deltaIfnb* N2A media (Fig. S6L), wild-type neurons treated with H<sub>2</sub>O<sub>2</sub> (Fig. 6L), or EVs from *Ifnb*<sup>-/-</sup> CN media (Fig. 6M). Accordingly, knockdown of Rps3 reduced toxicity induced by CM from *deltaIfnb* N2A cells in WT N2As, as shown by decreased MTT (Fig. 6N).

In conclusion, we identified TLR4 activator, Rps3 as an important cofactor which recognizes and binds the damaged mtDNA extruded outside mitochondria. Damaged mtDNA-Rps3 complexes are then extruded extra-neuronally, at least partly in EVs which in turn participate in the neurodegenerative pathology and propagation of PDD-like disease via activation of TLR pathways (Fig. S7).

## DISCUSSION

We have previously demonstrated that disruption of the IFN $\beta$ -IFNAR1 signalling pathway is associated and can cause development of PD with dementia [27, 28, 30]. In the current study, we identified mtDNA deletions in a hotspot in complex I respiratory

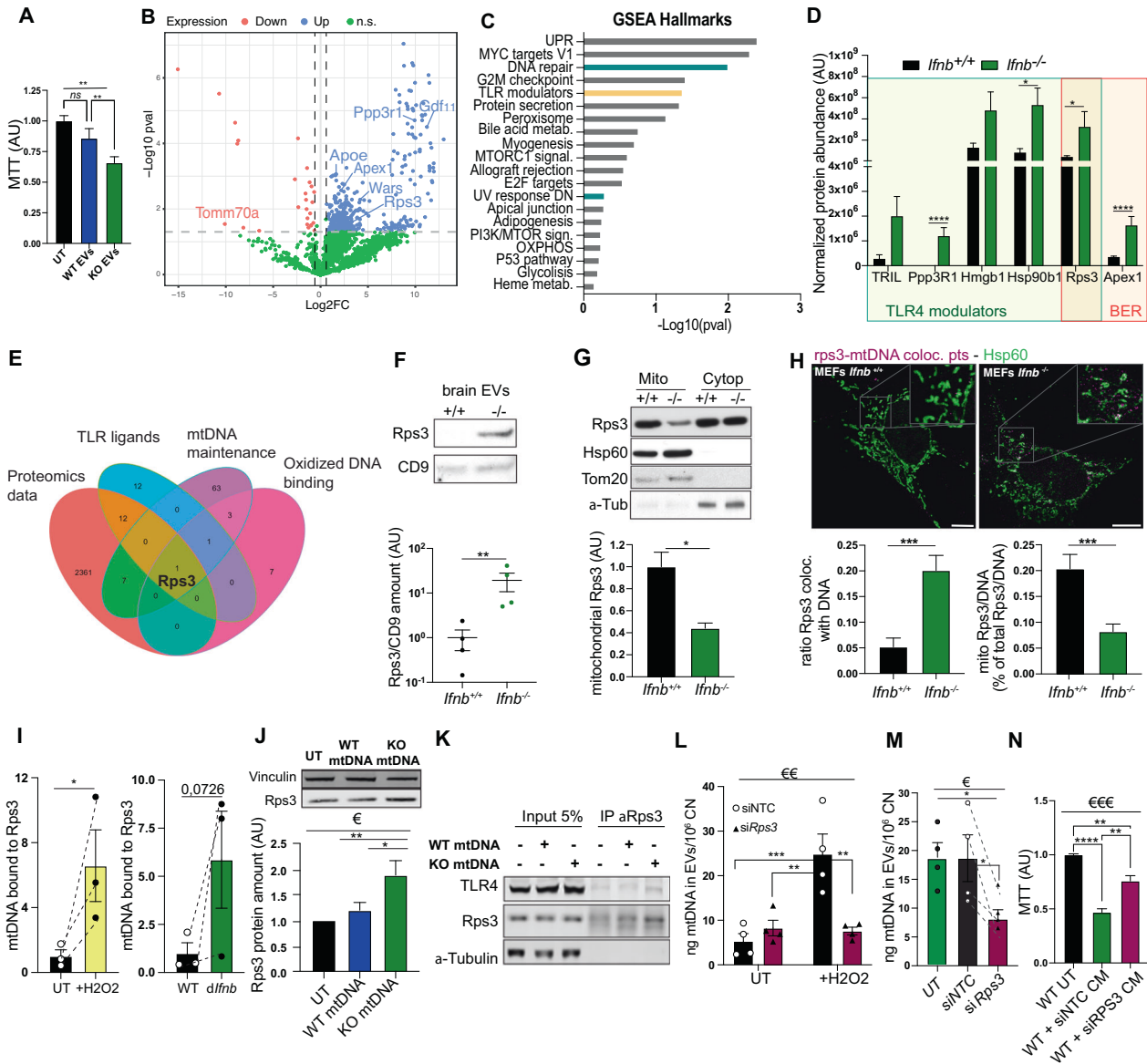


**Fig. 6** TLR4 activator Rps3 recognizes damaged mtDNA and is essential for its extrusion in EVs. **A** Metabolic activity of CN upon treatment with EVs purified for either wild type or *lfnb*<sup>-/-</sup> CN CM. *N* = 4. **B** Volcano plot of proteins differentially expressed in EVs purified from wild-type and *lfnb*<sup>-/-</sup> CN. DEP analysis of *N* = 3. **C** Top GSEA pathways dysregulated in *lfnb*<sup>-/-</sup> EVs. **D** Normalized abundances of some TLR4 modulators and BER proteins found in *lfnb*<sup>-/-</sup> EVs. **E** Venn Diagram of the common proteins between our dataset, TLR4 ligands, mitochondrial DNA maintenance and oxidized DNA binding pathways. **F** Immunoblot for Rps3 and EV marker CD9 in EVs purified from wild-type and *lfnb*<sup>-/-</sup> mouse brains. **G** Cellular fractionation of CNs followed by immunoblot for Rps3. Hsp60 and Tom20 indicate the mitochondrial fraction and  $\alpha$ -tubulin the cytoplasmic fraction. **H** Rps3/DNA colocalization points extracted from immunofluorescence for DNA, Rps3 and Hsp60 (mitochondria) with quantifications in *lfnb*<sup>+/+</sup> and *lfnb*<sup>-/-</sup> MEFs. *N* = 3. **I** Amount of mtDNA CoIP with Rps3 in N2A cells with or without oxidative stress induced by H<sub>2</sub>O<sub>2</sub> or by lack of *lfnb*. *N* = 3. **J** Immunoblot showing the amount of Rps3 in wild-type CNs treated with either WT or KO mtDNA. *N* = 3. **K** Immunoblotting showing CoIP of TLR4 with Rps3 in N2A cells untreated or treated with WTmtDNA or KOmtDNA. **L** Quantified mtDNA in EVs purified from WT CN  $\pm$  H<sub>2</sub>O<sub>2</sub> treatment with or without Rps3 knock-down. **M** Amount of mtDNA quantified in EVs purified from *lfnb*<sup>-/-</sup> CN with or without Rps3 knock-down. *N* = 4. **N** Metabolic activity assessed by MTT assay in wild-type cell treated with CM from *lfnb* N2A with or without knock-down for Rps3, *N* = 3. For all graphs, 1 dot means 1 individual animal. €€ means *p* < 0.01 and €€€ *p* < 0.001 by ordinary one-way ANOVA, Kruskal–Wallis ANOVA if distribution did not show Gaussian distribution (Shapiro–Wilk test) or Brown–Forsythe ANOVA if distribution showed SD differences (Bartlett’s test). \* means *p* < 0.05 and \*\* *p* < 0.01, by post-hoc unpaired *t*-test.

chain subunits associated with dysregulated oxidative stress, cytosolic DNA damages and sensing pathways in cohorts of sporadic PD and PDD, in the same cohorts in which we previously reported type I IFN disruption as a top dysregulated signaling pathway [28]. These mtDNA alterations may result from the impairment of mitochondrial fission, autophagy, and mitophagy, as observed when the IFN $\beta$ -IFNAR1 signaling pathway is disrupted [27, 28, 30]. Consistently, previous studies have demonstrated that

mtDNA damages are managed through the process of mitophagy [58, 59], or alternatively released via cell-free mtDNA or enclosed within EVs [60].

To investigate the relevance of mtDNA damages in PD pathology, we utilized spontaneous mice PDD models where IFN $\beta$  or IFNAR genes are deleted [27, 28, 30]. We observed that lack of endogenous neuronal IFN $\beta$ -IFNAR signaling causes altered mtDNA, harboring sequence variations and oxidative damages.

Damaged mtDNA is in turn extruded from IFN $\beta$ /IFNAR knock-out neurons partly through EVs causing and spreading neurotoxicity. Moreover, we established that, although the damages in mtDNA and their subsequent release from neurons occurs only when the endogenous IFN $\beta$ -IFNAR signaling is defective, their “infectious-like” spread of the pathology is IFN $\beta$ /IFNAR-independent. Furthermore, we identified that the damaged mtDNA extrusion is dependent on its recognition by Rps3, a protein reported to be involved in oxidative DNA repair [61] and in TLR4 activation [32], but with no previously known role in the extrusion of damaged mtDNA and neurodegeneration. Importantly, we demonstrated that the damaged mtDNA extruded from neurons is neurotoxic, notably through the coactivation of TLR9 and TLR4 which direct different molecular events. Our results established that while TLR9-dependent sensing is involved in neuronal mitochondrial oxidative stress, TLR4 activation contributes to neuronal cell-death. Of note, we did not observe a role for cGAS-STING pathway, one of the earlier suggested main players [62–64], in our reported neuronal pathologies.

Although an increased presence of mtDNA mutations in PD patients is reported [14, 19, 65], the functions of extruded and circulating mtDNA and their relationship to physiological and pathological conditions in the context of PD remain a subject of intense debate, with conflicting findings reported in various models [65–68]. Remarkably, the specific characteristics of mtDNA that are released and subsequently extruded extracellularly, as well as their *in vivo* implications for the propagation of PDD pathology, have not been thoroughly investigated. Macrophages are reported to fragment and release oxidized mtDNA via VDAC pores [69] and not via MDVs, thus distinct from the extrusion mechanism observed here in post-mitotic neurons.

Significantly, we demonstrated that damaged mtDNA, resulting from impaired neuronal IFN $\beta$ -IFNAR signaling, does not only induce PDD-like pathology upon injection into healthy animals, including causing motor and cognitive deficits,  $\alpha$ -synuclein accumulation, and neuronal loss, it also triggers the spread of the pathology to other brain regions in an “infectious-like manner”. The precise mechanisms of this spread are still to be elucidated, but the impact of damaged mtDNA on TLR9-mediated mitochondrial membrane potential reduction and oxidative stress increase suggests that damaged mtDNA could spread mitochondrial dysfunction to neighbouring healthy neurons. This is supported by the observed increase in neuronal oxDJ1, not only at the injection site but also in distant brain regions. Interestingly, previous studies have demonstrated that oxidative stress promotes prion-like protein aggregation [70].

Our findings indicate that the neuronal pathology induced by damaged mtDNA involves the coactivation of TLR9 and TLR4. We observed increased expression of both receptors in the transcriptome of PDD patients, which was further verified in another cohort of PDD patients, mouse brains injected with damaged KOmtDNA, and primary neurons treated with damaged KOmtDNA. Surprisingly, *Tlr4* showed higher upregulation upon treatment with damaged mtDNA compared to WTmtDNA. While TLR9 has been previously reported to recognize unmethylated CpG motifs from mtDNA [50, 51], the association of TLR4 with mtDNA sensing is elusive. Previous studies had suggested the involvement of TLR4 in PD pathology [71, 72], but primarily linked to microglia activation by  $\alpha$ -synuclein [73, 74]. However, its association with mtDNA pathology and its role in neuronal death associated with PDD had not been demonstrated. In our study, we identified Rps3 as a key mediator of TLR4 activation in response to damaged mtDNA in neurons. Rps3 specifically recognizes oxidative damages on mtDNA and directly binds to TLR4. It plays a crucial role in nuDNA and mtDNA maintenance during oxidative stress in mammalian cells, including neurons [56, 57, 75–77]. We show that Rps3 is essential for the recognition of damaged mtDNA in neurons and its extrusion from mitochondria in EVs. This

alternative mechanism is particularly important in neurons with defective mitophagy, such as *lfnb*<sup>-/-</sup>/*lfnar1*<sup>-/-</sup> neurons. This would restrict cytosolic mtDNA leakage and subsequent cGAS activation, thereby preventing an inflammatory response [58]. However, if damaged mtDNA is released extracellularly, in cell-free form or enclosed within EVs, it may cause an infectious-like pathology upon uptake by healthy neurons.

Our data reveal a distinct role of damaged mtDNA in neurotoxicity and the spread of an infectious PDD-like pathology. This process involves the participation of EVs and the key players Rps3-TLR4 and TLR9, operating independently of cGAS and IFN $\beta$ -IFNAR signaling. The understanding of damaged mtDNA/Rps3-mediated neurodegeneration holds promises in elucidating the mechanisms underlying the propagation of Parkinson's pathology throughout the brain and its progression to dementia. These insights may pave the way for innovative treatment strategies and monitoring approaches for Parkinson's disease.

## DATA AVAILABILITY

The mass spectrometry proteomics data have been deposited to the ProteomeX-change Consortium via the PRIDE partner repository with the dataset identifier PXD038362.

## REFERENCES

- Mhyre TR, Boyd JT, Hamill RW, Maguire-Zeiss KA. Parkinson's disease. *Subcell Biochem.* 2012;65:389–455.
- Maday S, Twelvetrees AE, Moughamian AJ, Holzbaur EL. Axonal transport: cargo-specific mechanisms of motility and regulation. *Neuron* 2014;84:292–309.
- Crotty P, Sangrey T, Levy WB. Metabolic energy cost of action potential velocity. *J Neurophysiol.* 2006;96:1237–46.
- Attwell D, Laughlin SB. An energy budget for signaling in the grey matter of the brain. *J Cereb Blood Flow Metab.* 2001;21:1133–45.
- Polymeropoulos MH, Lavedan C, Leroy E, Ide SE, Dehejia A, Dutra A, et al. Mutation in the alpha-synuclein gene identified in families with Parkinson's disease. *Science* 1997;276:2045–7.
- Kitada T, Asakawa S, Hattori N, Matsumine H, Yamamura Y, Minoshima S, et al. Mutations in the parkin gene cause autosomal recessive juvenile parkinsonism. *Nature* 1998;392:605–8.
- Zimprich A, Biskup S, Leitner P, Lichtner P, Farrer M, Lincoln S, et al. Mutations in LRRK2 cause autosomal-dominant parkinsonism with pleomorphic pathology. *Neuron* 2004;44:601–7.
- Zimprich A, Muller-Myhsok B, Farrer M, Leitner P, Sharma M, Hulihan M, et al. The PARK8 locus in autosomal dominant parkinsonism: confirmation of linkage and further delineation of the disease-containing interval. *Am J Hum Genet.* 2004;74:11–9.
- Langston JW, Schule B, Rees L, Nichols RJ, Barlow C. Multisystem Lewy body disease and the other parkinsonian disorders. *Nat Genet.* 2015;47:1378–84.
- Bonifati V, Rizzu P, van Baren MJ, Schaap O, Breedveld GJ, Krieger E, et al. Mutations in the DJ-1 gene associated with autosomal recessive early-onset parkinsonism. *Science* 2003;299:256–9.
- Sazer S, Sherwood SW. Mitochondrial growth and DNA synthesis occur in the absence of nuclear DNA replication in fission yeast. *J Cell Sci.* 1990;97:509–16.
- Chapman J, Ng YS, Nicholls TJ. The Maintenance of Mitochondrial DNA Integrity and Dynamics by Mitochondrial Membranes. *Life (Basel).* 2020;10:164.
- Goldsmith J, Ordureau A, Harper JW, Holzbaur ELF. Brain-derived autophagosome profiling reveals the engulfment of nucleoid-enriched mitochondrial fragments by basal autophagy in neurons. *Neuron* 2022;110:967–76.e8.
- Bender A, Krishnan KJ, Morris CM, Taylor GA, Reeve AK, Perry RH, et al. High levels of mitochondrial DNA deletions in substantia nigra neurons in aging and Parkinson disease. *Nat Genet.* 2006;38:515–7.
- Nido GS, Dolle C, Flices I, Tuppen HA, Alves G, Tysnes OB, et al. Ultradeep mapping of neuronal mitochondrial deletions in Parkinson's disease. *Neurobiol Aging.* 2018;63:120–7.
- Blackinton J, Kumaran R, van der Brug MP, Ahmad R, Olson L, Galter D, et al. Post-transcriptional regulation of mRNA associated with DJ-1 in sporadic Parkinson disease. *Neurosci Lett.* 2009;452:8–11.
- Papa S, Petruzzella V, Scacco S, Sardaneli AM, Iuso A, Panelli D, et al. Pathogenic mechanisms in hereditary dysfunctions of complex I of the respiratory chain in neurological diseases. *Biochim Biophys Acta.* 2009;1787:502–17.
- Kapsa RM, Jean-Francois MJ, Lertrit P, Weng S, Siregar N, Ojaimi J, et al. Mitochondrial DNA polymorphism in substantia nigra. *J Neurol Sci.* 1996;144:204–11.

19. Lin MT, Cantuti-Castelvetri I, Zheng K, Jackson KE, Tan YB, Arzberger T, et al. Somatic mitochondrial DNA mutations in early Parkinson and incidental Lewy body disease. *Ann Neurol*. 2012;71:850–4.
20. Reeve AK, Krishnan KJ, Turnbull DM. Age related mitochondrial degenerative disorders in humans. *Biotechnol J*. 2008;3:750–6.
21. Ekstrand MI, Terzioglu M, Galter D, Zhu S, Hofstetter C, Lindqvist E, et al. Progressive parkinsonism in mice with respiratory-chain-deficient dopamine neurons. *Proc Natl Acad Sci USA*. 2007;104:1325–30.
22. Hwang M, Bergmann CC. Neuronal Ablation of Alpha/Beta Interferon (IFN-alpha/beta) Signaling Exacerbates Central Nervous System Viral Dissemination and Impairs IFN-gamma Responsiveness in Microglia/Macrophages. *J Virol*. 2020;94:e00422–20.
23. Svennerholm B, Ziegler R, Lycke E. Herpes simplex virus infection of the rat sensory neuron. Effects of interferon on cultured cells. *Arch Virol*. 1989;104:153–6.
24. Jakimovski D, Kolb C, Ramanathan M, Zivadinov R, Weinstock-Guttman B. Interferon beta for Multiple Sclerosis. *Cold Spring Harb Perspect Med*. 2018;8:a032003.
25. Inacio AR, Liu Y, Clausen BH, Svensson M, Kucharz K, Yang Y, et al. Endogenous IFN-beta signaling exerts anti-inflammatory actions in experimentally induced focal cerebral ischemia. *J Neuroinflamm*. 2015;12:211.
26. Liu H, Xin L, Chan BP, Teoh R, Tang BL, Tan YH. Interferon-beta administration confers a beneficial outcome in a rabbit model of thromboembolic cerebral ischemia. *Neurosci Lett*. 2002;327:146–8.
27. Ejlerskov P, Hultberg JG, Wang J, Carlsson R, Ambjorn M, Kuss M, et al. Lack of Neuronal IFN-beta-IFNAR Causes Lewy Body- and Parkinson's Disease-like Dementia. *Cell* 2015;163:324–39.
28. Magalhaes J, Tresse E, Ejlerskov P, Hu E, Liu Y, Marin A, et al. PIAS2-mediated blockade of IFN-beta signaling: a basis for sporadic Parkinson disease dementia. *Mol Psychiatry*. 2021;26:6083–99.
29. Villanueva EB, Tresse E, Liu Y, Duarte JN, Jimenez-Duran G, Ejlerskov P, et al. Neuronal TNFalpha, not alpha-syn, underlies PDD-like disease progression in IFNbeta-KO mice. *Ann Neurol*. 2021;90:789–807.
30. Tresse E, Riera-Ponsati L, Jaberri E, Sew WQG, Ruscher K, Issazadeh-Navikas S. IFN-beta rescues neurodegeneration by regulating mitochondrial fission via STAT5, PGAM5, and Drp1. *EMBO J*. 2021;40:e106868.
31. Shahni R, Cale CM, Anderson G, Osellame LD, Hambleton S, Jacques TS, et al. Signal transducer and activator of transcription 2 deficiency is a novel disorder of mitochondrial fission. *Brain* 2015;138:2834–46.
32. Park HJ, Jang GY, Kim YS, Park JH, Lee SE, Vo MC, et al. A novel TLR4 binding protein, 40S ribosomal protein S3, has potential utility as an adjuvant in a dendritic cell-based vaccine. *J Immunother Cancer*. 2019;7:60.
33. Li L, Ji B, Zhao T, Cui X, Chen J, Wang Z. The structural changes of gray matter in Parkinson disease patients with mild cognitive impairments. *PLoS ONE*. 2022;17:e0269787.
34. Pereira JB, Svenningsson P, Weintraub D, Bronnick K, Lebedev A, Westman E, et al. Initial cognitive decline is associated with cortical thinning in early Parkinson disease. *Neurology* 2014;82:2017–25.
35. Jaberri E, Tresse E, Gronbaek K, Weischenfeldt J, Issazadeh-Navikas S. Identification of unique and shared mitochondrial DNA mutations in neurodegeneration and cancer by single-cell mitochondrial DNA structural variation sequencing (MitoSV-seq). *EBioMedicine* 2020;57:102868.
36. Perez-Gonzalez R, Gauthier SA, Kumar A, Saito M, Saito M, Levy E. A Method for Isolation of Extracellular Vesicles and Characterization of Exosomes from Brain Extracellular Space. *Methods Mol Biol*. 2017;1545:139–51.
37. Kim Y, Kim HD, Youn B, Park YG, Kim J. Ribosomal protein S3 is secreted as a homodimer in cancer cells. *Biochem Biophys Res Commun*. 2013;441:805–8.
38. Phillips NR, Sprouse ML, Roby RK. Simultaneous quantification of mitochondrial DNA copy number and deletion ratio: a multiplex real-time PCR assay. *Sci Rep*. 2014;4:3887.
39. Ibarretxe-Bilbao N, Ramirez-Ruiz B, Tolosa E, Marti MJ, Valldeoriola F, Bargallo N, et al. Hippocampal head atrophy predominance in Parkinson's disease with hallucinations and with dementia. *J Neurol*. 2008;255:1324–31.
40. Zarei M, Ibarretxe-Bilbao N, Compta Y, Hough M, Junque C, Bargallo N, et al. Cortical thinning is associated with disease stages and dementia in Parkinson's disease. *J Neurol Neurosurg Psychiatry*. 2013;84:875–81.
41. Bette S, Zimmermann U, Wissinger B, Knipper M. OPA1, the disease gene for optic atrophy type Kjer, is expressed in the inner ear. *Histochem Cell Biol*. 2007;128:421–30.
42. Paulin-Levasseur M, Chen G, Lariviere C. The 2G2 antibody recognizes an acidic 110-kDa human mitochondrial protein. *Histochem J*. 1998;30:617–25.
43. Soubannier V, McLelland GL, Zunino R, Braschi E, Rippstein P, Fon EA, et al. A vesicular transport pathway shuttles cargo from mitochondria to lysosomes. *Curr Biol*. 2012;22:135–41.
44. MacMahon Copas AN, McComish SF, Fletcher JM, Caldwell MA. The Pathogenesis of Parkinson's Disease: A Complex Interplay Between Astrocytes, Microglia, and T Lymphocytes? *Front Neurol*. 2021;12:666737.
45. Huang LS, Hong Z, Wu W, Xiong S, Zhong M, Gao X, et al. mtDNA Activates cGAS Signaling and Suppresses the YAP-Mediated Endothelial Cell Proliferation Program to Promote Inflammatory Injury. *Immunity* 2020;52:475–86.e5.
46. Bueno M, Zank D, Buendia-Roldan I, Fiedler K, Mays BG, Alvarez D, et al. PINK1 attenuates mtDNA release in alveolar epithelial cells and TLR9 mediated profibrotic responses. *PLoS ONE*. 2019;14:e0218003.
47. Aarsland D, Kurz MW. The epidemiology of dementia associated with Parkinson disease. *J Neurol Sci*. 2010;289:18–22.
48. Doty RL. Olfaction in Parkinson's disease and related disorders. *Neurobiol Dis*. 2012;46:527–52.
49. Höglinger GU, Alvarez-Fischer D, Arias-Carrion O, Djufri M, Windolph A, Keber U, et al. A new dopaminergic nigro-olfactory projection. *Acta Neuropathol*. 2015;130:333–48.
50. Hemmi H, Takeuchi O, Kawai T, Kaisho T, Sato S, Sanjo H, et al. A Toll-like receptor recognizes bacterial DNA. *Nature* 2000;408:740–5.
51. Zhang Y, Lee AS, Shamel A, Geng X, Finegood D, Santamaria P, et al. TLR9 blockade inhibits activation of diabetogenic CD8+ T cells and delays autoimmune diabetes. *J Immunol*. 2010;184:5645–53.
52. Caielli S, Conforti-Andreoni C, Di Pietro C, Usulli V, Badami E, Malosio ML, et al. On/off TLR signaling decides proinflammatory or tolerogenic dendritic cell maturation upon CD1d-mediated interaction with invariant NKT cells. *J Immunol*. 2010;185:7317–29.
53. Shi M, Liu C, Cook TJ, Bullock KM, Zhao Y, Ginghina C, et al. Plasma exosomal alpha-synuclein is likely CNS-derived and increased in Parkinson's disease. *Acta Neuropathol*. 2014;128:639–50.
54. Kato H, Lu Q, Rapaport D, Kozjak-Pavlovic V. Tom70 is essential for PINK1 import into mitochondria. *PLoS ONE*. 2013;8:e58435.
55. Todkar K, Chikhi L, Desjardins V, El-Mortada F, Pepin G, Germain M. Selective packaging of mitochondrial proteins into extracellular vesicles prevents the release of mitochondrial DAMPs. *Nat Commun*. 2021;12:1971.
56. Hegde V, Wang M, Deutsch WA. Human ribosomal protein S3 interacts with DNA base excision repair proteins hAPE/Ref-1 and hOGG1. *Biochemistry*. 2004;43:14211–7.
57. Hegde V, Yadavilli S, McLaughlin LD, Deutsch WA. DNA repair efficiency in transgenic mice over expressing ribosomal protein S3. *Mutat Res*. 2009;666:16–22.
58. Wasner K, Smajic S, Ghelfi J, Delcambre S, Prada-Medina CA, Knappe E, et al. Parkin Deficiency Impairs Mitochondrial DNA Dynamics and Propagates Inflammation. *Mov Disord*. 2022;37:1405–15.
59. Palozzi JM, Hurd TR. The role of programmed mitophagy in germline mitochondrial DNA quality control. *Autophagy*. 2023;19:2817–18.
60. De Gaetano A, Solodka K, Zanini G, Selleri V, Mattioli AV, Nasi M, et al. Molecular Mechanisms of mtDNA-Mediated Inflammation. *Cells*. 2021;26:10:2898.
61. Hegde AN. Ubiquitin-proteasome-mediated local protein degradation and synaptic plasticity. *Prog Neurobiol*. 2004;73:311–57.
62. Caielli S, Athale S, Domic B, Murat E, Chandra M, Bancheau R, et al. Oxidized mitochondrial nucleoids released by neutrophils drive type I interferon production in human lupus. *J Exp Med*. 2016;213:697–713.
63. Fang C, Mo F, Liu L, Du J, Luo M, Men K, et al. Oxidized mitochondrial DNA sensing by STING signaling promotes the antitumor effect of an irradiated immunogenic cancer cell vaccine. *Cell Mol Immunol*. 2021;18:2211–23.
64. Fang R, Jiang Q, Guan Y, Gao P, Zhang R, Zhao Z, et al. Golgi apparatus-synthesized sulfated glycosaminoglycans mediate polymerization and activation of the cGAMP sensor STING. *Immunity* 2021;54:962–75.e8.
65. Dolle C, Flonès I, Nido GS, Miletic H, Osuagwu N, Kristoffersen S, et al. Defective mitochondrial DNA homeostasis in the substantia nigra in Parkinson disease. *Nat Commun*. 2016;7:13548.
66. Lowes H, Pyle A, Santibanez-Koref M, Hudson G. Circulating cell-free mitochondrial DNA levels in Parkinson's disease are influenced by treatment. *Mol Neurodegener*. 2020;15:10.
67. Pyle A, Lowes H, Brennan R, Kurzawa-Akanbi M, Yarnall A, Burn D, et al. Reduced mitochondrial DNA is not a biomarker of depression in Parkinson's disease. *Mov Disord*. 2016;31:1923–4.
68. Sliter DA, Martinez J, Hao L, Chen X, Sun N, Fischer TD, et al. Parkin and PINK1 mitigate STING-induced inflammation. *Nature* 2018;561:258–62.
69. Xian H, Watari K, Sanchez-Lopez E, Offenberger J, Onyuru J, Sampath H, et al. Oxidized DNA fragments exit mitochondria via mPTP- and VDAC-dependent channels to activate NLRP3 inflammasome and interferon signaling. *Immunity* 2022;55:1370–85.e8.
70. Scudamore O, Ciosek T. Increased Oxidative Stress Exacerbates alpha-Synuclein Aggregation In Vivo. *J Neuropathol Exp Neurol*. 2018;77:443–53.
71. Kouli A, Horne CB, Williams-Gray CH. Toll-like receptors and their therapeutic potential in Parkinson's disease and alpha-synucleinopathies. *Brain Behav Immun*. 2019;81:41–51.

72. Perez-Pardo P, Dodiya HB, Engen PA, Forsyth CB, Huschens AM, Shaikh M, et al. Role of TLR4 in the gut-brain axis in Parkinson's disease: a translational study from men to mice. *Gut* 2019;68:829–43.
73. Duffy MF, Collier TJ, Patterson JR, Kemp CJ, Luk KC, Tansey MG, et al. Lewy body-like alpha-synuclein inclusions trigger reactive microgliosis prior to nigral degeneration. *J Neuroinflamm*. 2018;15:129.
74. Fellner L, Irschick R, Schanda K, Reindl M, Klimaschewski L, Poewe W, et al. Toll-like receptor 4 is required for alpha-synuclein dependent activation of microglia and astroglia. *Glia* 2013;61:349–60.
75. Kim Y, Kim HD, Kim J. Cytoplasmic ribosomal protein S3 (rpS3) plays a pivotal role in mitochondrial DNA damage surveillance. *Biochim Biophys Acta*. 2013;1833:2943–52.
76. Kim J, Chubatsu LS, Admon A, Stahl J, Fellous R, Linn S. Implication of mammalian ribosomal protein S3 in the processing of DNA damage. *J Biol Chem*. 1995;270:13620–9.
77. Ahn EH, Kim DW, Shin MJ, Kim YN, Kim HR, Woo SJ, et al. PEP-1-ribosomal protein S3 protects dopaminergic neurons in an MPTP-induced Parkinson's disease mouse model. *Free Radic Biol Med*. 2013;55:36–45.

## ACKNOWLEDGEMENTS

This project received funding from the European Union's Horizon 2020 Research and Innovation Program under Marie Skłodowska-Curie Grant No. 703217, the Lundbeck Foundation (R223-2016-849 and R359-2020-2658), and the Danish Council for Independent Research-Medicine (DFF-6110-0065 and DFF-2034-00015B) to SI-N. Proteomics was performed at the proteomics core at DTU Bioengineering. We thank the HT-Cell based screen platform at Biotech Research and Innovation Centre at University of Copenhagen for High content imaging and analysis. We thank Carsten Friis Rundsted for bioinformatics analysis of microarrays and Xinchun Nie for help to produce the Venn diagram.

## AUTHOR CONTRIBUTIONS

ET, JM, GS, MC, LR-P, EH developed and conducted the experiments. ET and SI-N interpreted the results. OK performed the electron microscopy studies. SA provided human samples. NF proceeded with animal injections and established the double blinded system. EJ performed the MitoSVseq experiments and analysis. JM performed proteomics of EVs and their analysis. ET wrote the first draft of the paper. SI-N developed the concept and secured funding. All authors read and contributed to the final paper.

## FUNDING

Open access funding provided by Royal Library, Copenhagen University Library.

## COMPETING INTERESTS

The authors declare no competing interests.

## ETHICS APPROVAL

All experiments have been performed according to ethical and health and safety regulation in place in Denmark and Germany.

## ADDITIONAL INFORMATION

**Supplementary information** The online version contains supplementary material available at <https://doi.org/10.1038/s41380-023-02251-4>.

**Correspondence** and requests for materials should be addressed to Shohreh Issazadeh-Navikas.

**Reprints and permission information** is available at <http://www.nature.com/reprints>

**Publisher's note** Springer Nature remains neutral with regard to jurisdictional claims in published maps and institutional affiliations.



**Open Access** This article is licensed under a Creative Commons Attribution 4.0 International License, which permits use, sharing, adaptation, distribution and reproduction in any medium or format, as long as you give appropriate credit to the original author(s) and the source, provide a link to the Creative Commons licence, and indicate if changes were made. The images or other third party material in this article are included in the article's Creative Commons licence, unless indicated otherwise in a credit line to the material. If material is not included in the article's Creative Commons licence and your intended use is not permitted by statutory regulation or exceeds the permitted use, you will need to obtain permission directly from the copyright holder. To view a copy of this licence, visit <http://creativecommons.org/licenses/by/4.0/>.

© The Author(s) 2023